Environmental Science: Atmospheres

ROYAL SOCIETY OF CHEMISTRY

PAPER

View Article Online
View Journal

Cite this: DOI: 10.1039/d6ea00035e

A conceptual framework for the influence of water activity parameterization on hygroscopic growth and cloud droplet activation in aerosols containing strong nonionic surfactants

Alison Bain *

Discrepancies between observations of cloud droplet number concentrations during field studies and those predicted from Köhler theory suggest that surface-active organics may impact hygroscopic growth. The surface-active material that partitions to the droplet–air interface can reduce the surface tension, lowering the barrier to cloud droplet activation. However, when the surface-active material partitions to the interface, it also increases the droplet water activity, having the opposite effect on cloud droplet activation. Although much effort has been focused on accurately describing the size- and composition-dependent surface tension, the influence of surface-active organics on water activity has received far less attention. Here, the impact of the description of water activity during hygroscopic growth and eventual cloud droplet activation is investigated. In AIOMFAC (Aerosol Inorganic–Organic Mixtures Functional groups Activity Coefficients), two subgroup descriptions (ether–alkyl and oxyethylene) of the strong nonionic surfactants Triton X-100 and Tween20 and their mixtures with NaCl are used to calculate water activity for Köhler calculations. Although for aerosols with low and medium organic content, the two AIOMFAC descriptions of the surfactants provide equivalent estimates of the critical supersaturation and radius, under high surfactant conditions, the oxyethylene subgroup description predicts a lower critical supersaturation than the ether–alkyl subgroup description. Under high surfactant conditions, the oxyethylene subgroup also provides better agreement with available literature data for critical supersaturation.

Received 5th March 2026
Accepted 20th May 2026

DOI: 10.1039/d6ea00035e

rsc.li/esatmospheres

Environmental significance

An accurate understanding of the number of aerosol particles that will become cloud droplets under a set of atmospheric conditions is necessary to understand the aerosol indirect effect on climate. Field observations have found that traditional Köhler calculations can underpredict cloud condensation nuclei concentration. The partitioning of surfactants, which influences both aerosol surface tension and water activity, has been suggested to explain this discrepancy. The influence of the description of water activity during surfactant partitioning has received little attention compared to surface tension. Here, the influence of the description of water activity during hygroscopic growth is investigated for aerosols containing nonionic surfactants. Under high surfactant concentrations, the description of water activity plays a role in the predicted activation barrier.

Introduction

Aerosol particles suspended in the atmosphere can interact with climate by directly scattering and absorbing solar radiation and by altering cloud microphysics. Aerosol particles can act as seeds for cloud droplet formation. The eventual formation of clouds depends on many factors including the supersaturation level of the atmosphere, the number concentration of aerosol particles as well as the aerosol population size distribution and chemical composition.[1,2] Köhler theory, which takes into account both the vapor pressure over the droplet due to dissolved solute and the surface curvature effect, is typically used to predict the activation of aerosol particles into cloud droplets.[1,2] However, discrepancies exist between predictions of cloud condensation nuclei (CCN) concentrations and the number of cloud droplets observed during field campaigns.[3–5] Generally, these discrepancies are more pronounced at smaller aerosol dry sizes.[3–6]

Atmospheric aerosol particles are composed of complex mixtures of salts (*e.g.*, NaCl and $(NH_4)_2SO_4$) as well as a wide array of organic molecules.[7,8] The ratio of salts to organics, particularly in sea spray aerosols, has been observed to strongly depend on size, owing to different aerosol generation pathways.[9–11] Many organic molecules have some surface activity (*i.e.*, they partition to the droplet–air interface).[12,13] This

Department of Chemistry, Oregon State University, Corvallis, OR, 97331, USA. E-mail: alison.bain@oregonstate.edu

surface active material has been characterized in a variety of aerosol samples[11,14–17] and shown to be formed in chemical reactions in model aerosol systems.[18] Sea spray aerosols also include strongly surface-active materials (surfactants) generated in the sea surface microlayer.[19,20]

Recently, the impact of surfactant partitioning on aerosol surface tension and its role in cloud droplet activation have been investigated.[21–33] Laboratory measurements of surface tension at the single particle level help elucidate the effect of surface-area-to-volume ratio on the partitioning of strong surfactants.[34–41] Surfactants partitioning to the air–droplet interface lower the surface tension, thereby reducing the barrier to cloud droplet activation. However, removal of surfactants from the droplet bulk also affects the water activity. Reducing the solute in the droplet bulk increases water activity, which has an opposite effect on the cloud droplet activation barrier.[42]

Systematic laboratory measurements of hygroscopic growth and cloud droplet activation for mixtures of salts and soluble surfactants in aerosol particles provide information about the combined result of these two counteracting effects. In optically trapped micron-sized droplets, the subsaturated hygroscopic growth of droplets containing surfactants and NaCl has been reported to be reduced compared to droplets containing only NaCl.[43,44] Bramblett and Frossard used humidified tandem differential mobility analyzer (HTDMA) measurements of 100 nm dry diameter aerosols to measure the hygroscopic growth of particles containing NaCl and a range of surfactants (nonionic, anionic, or cationic) in a 2 : 1 mass ratio. Their results show a reduction in hygroscopic growth of particles containing surfactants compared to pure NaCl particles at subsaturated relative humidities.[45] The hygroscopic growth of particles containing NaCl and ionic surfactants with a dry size less than 30 nm has also been measured using HTDMA.[46,47] These studies observed a decrease in hygroscopic growth with increasing surfactant fraction under subsaturated conditions. Petters and Petters measured CCN activity of accumulation mode aerosol particles containing mixtures of strong surfactants and salts.[12] They found that aerosol hygroscopicity under supersaturated conditions decreases as the surfactant volume fraction of the dry aerosol increases.[12] Overall, soluble surfactants have been found to decrease the hygroscopic growth of aerosols across a range of surfactant properties and dry aerosol sizes, but the interplay between the surfactant impact on surface tension and water activity cannot be decoupled.

Compared to surface tension, the impact of surface-active material on aerosol water activity has received less attention. κ-Köhler theory is commonly used to approximate water activity, requiring only knowledge of the dry and wet diameters in addition to the hygroscopicity constant κ for the aerosol, which can be calculated from volume fractions of the different aerosol components.[48] While often treated as a constant, κ generally varies with water activity.[49,50] Alternatively, parameterizations of water activities measured for solutions containing surface-active material have been used as an input for Köhler calculations.[51] Solutions containing surface-active material have also been treated as ideal solutions (*i.e.*, assuming activity coefficients are equal to one).[24] Additionally, some work has used predictions of water activity from thermodynamic models such as UNIFAC (UNIQUAC Functional-group Activity Coefficients)[52] and AIOMFAC (Aerosol Inorganic–Organic Mixtures Functional groups Activity Coefficients).[5,22] Zhang *et al.* looked at the impact of surface tension and water activity on predictions of aerosol growth factor for droplets containing adipic acid (a sparingly soluble organic acid) and ammonium sulfate at different mass ratios.[52] Generally, a description of water activity that accounted for nonidealities was necessary to find agreement with high-humidity tandem differential mobility analyzer (HHTDMA) measurements.[52]

Recently, water activity measurements for solutions containing strong nonionic surfactants and their mixtures with NaCl were used to test water activity predictions of these solutions from AIOMFAC.[50] For surfactants containing PEG-like tails, the traditional approach using ether and alkyl groups to describe the tail provided poor agreement with measurements. An alternative oxyethylene subgroup approach was shown to better predict the macroscopic measurements. These two sets of model predictions generally agree at high water activities but deviate significantly under drier conditions. Additionally, the ether–alkyl subgroup approach indicates that a liquid–liquid phase separated (LLPS) state is likely to be stable under some relative humidity conditions. Here, the impact of the description of water activity during hygroscopic growth and cloud droplet activation, accounting for surfactant partitioning, is explored. Using model systems, a surfactant partitioning model is employed to predict the bulk droplet surfactant concentration. From this bulk concentration, the composition-dependent water activity predictions from AIOMFAC are compared using different subgroup descriptions of the surfactant and different assumptions when AIOMFAC returns a water activity greater than unity. These predictions are compared to CCN measurements available in the literature.

Experimental methods

NaCl (VWR BDH Chemicals), Triton X-100 (Sigma-Aldrich) and Tween20 (VWR BDH Chemicals) were used without any purification. Solutions were prepared using ultrapure water (18 MΩ cm) with mass ratios of 1 : 0.05, 1 : 0.1, 1 : 0.5, 1 : 1, and 1 : 2 surfactant : NaCl. The total solute concentration was varied to obtain surfactant concentration spanning orders of magnitude, from highly dilute to beyond the critical micelle concentration (CMC). Solutions were prepared with highly accurate concentrations using an analytical balance and analytical glassware (<0.15% uncertainty in concentration). Concentrated solutions were diluted to reach the low surfactant concentrations required for these measurements. The surface tension of the solutions was measured using the Wilhelmy plate method (DCATS, DataPhysics). All measurements were collected at room temperature, about 298 K, in triplicate, and average values are reported. Fig. S1 shows the surface tension data for the different surfactants and their mixtures with NaCl.

Surface tension data were fit with the Langmuir isotherm (eqn (1)) to determine the maximum surface excess, Γ_{max}, and the equilibrium partitioning constant, K_{eq}, which is defined as

the ratio of the surfactant adsorption and desorption rate constants at the interface. The Langmuir isotherm was fit only in the region where the surface tension decreases with increasing surfactant concentration, as the isotherm relates surface tension to fractional surface coverage.[53] When the interface is saturated with surfactant molecules, the surface tension remains constant as the surfactant concentration is further increased. This region was fit with a horizontal line to obtain the minimum achievable surface tension.

$$\sigma = \sigma_w + nRT\Gamma_{max} \times \ln\left(1 - \frac{K_{eq}c}{1 + K_{eq}c}\right) \quad (1)$$

In eqn (1), σ_w is the water solvent surface tension (72.8 mN m^{-1}), n is the van't Hoff factor, which is set equal to one for nonionic surfactants, c is the total surfactant concentration, R is the gas constant and T is the temperature.

For the nonionic surfactant–NaCl mixtures measured here, no trend in the shape of the surface tension isotherm or the minimum surface tension was observed as the ratio of NaCl was increased, indicating that the solubility of these surfactants is not greatly impacted by the addition of NaCl. The various ratios of surfactant to NaCl show no clear trend with mass ratio, and the datasets fall onto one line within the experimental variability. The overlaid binary surfactant–water data for Triton X-100 (ref. 21) and Tween20 (ref. 36) also fall within the spread of the NaCl-containing solution data. Since there is no clear trend in surface tension with NaCl mass fraction, a single set of Langmuir parameters and minimum surface tension was determined for each surfactant by fitting all of the surfactant data, including all of the NaCl mass ratios. Fit parameters are provided in Table 1, and the fitted lines are overlaid in Fig. S1.

Modeling

Water activity

AIOMFAC was used to calculate the water activity of solutions containing strong surfactants and NaCl.[50,54–56] The PEG-like tails of Triton X-100 and Tween20 can be described using either ether and alkyl groups or oxyethylene groups. Here, we calculate the water activities for mixtures of NaCl with each surfactant using both approaches. Each set of AIOMFAC calculations varied the mass ratio of NaCl to surfactant (in steps of 0.1) as well as the total mass fraction of solute (in steps of 0.01). All calculations were performed at 293 K. Interpolation was then used to infer the water activity between the calculated points. Fig. S2 shows the interpolated water activity over the surfactant–NaCl composition space for each surfactant and each subgroup description.

Table 1 Fitting parameters for surfactant solutions from surface tension measurements

Surfactant	Γ_{max} (mol m^{-2})	K_{eq} (m^3 mol^{-1})	σ_{min} (mN m^{-1})
Triton X-100	3.02×10^{-6}	1006.18	31.4
Tween20	2.47×10^{-6}	2930.85	36.9

Surface tension

The simple kinetic partitioning model[57] is used to calculate the effective bulk surfactant concentration (c_{eff}), accounting for a droplet's surface-area-to-volume ratio ($3/r$, where r is the droplets radius). This model has been previously shown to predict the surface tension of picolitre volume droplets containing surfactants and cosolutes as well as mixtures of surfactants, as accurately as or better than the widely used thermodynamic monolayer partitioning model.[35,37,38] Parameter f represents the ratio of the minimum bulk concentration required to reach a full surface coverage to the equilibrium partitioning constant, and parameter ζ represents the maximum fractional loss of surfactants to the interface once equilibrium is reached. Surfactant parameters Γ_{max} and K_{eq} are determined from Langmuir isotherm fits of macroscopic data (Table 1), and c is the total surfactant concentration.

$$\frac{c_{eff}}{c} = \frac{1}{2}\left(1 - \zeta - \frac{\zeta}{f}\right) + \frac{1}{2}\sqrt{\left(1 - \zeta - \frac{\zeta}{f}\right)^2 + 4\frac{\zeta}{f}} \quad (2)$$

$$\zeta = \frac{3\Gamma_{max}}{cr} \quad (3)$$

$$f = \frac{3K_{eq}\Gamma_{max}}{r} \quad (4)$$

Köhler calculations

Köhler theory incorporates the effects from surface curvature (Kelvin effect) and the solute (Raoult effect) to describe the relation between water activity (a_w, of the droplet bulk) and the saturation ratio (ratio of vapor pressure over the droplet, p_w, to the vapor pressure of pure water over a flat surface, p_0):[58]

$$\frac{p_w}{p_0} = a_w \times \exp\left(\frac{2\sigma\overline{V_w}}{rRT}\right). \quad (5)$$

Here, σ is the droplet's surface tension, $\overline{V_w}$ is the partial molar volume of water, r is the droplet radius, R is the gas constant and T is the temperature.

Near cloud droplet activation, solutes in a droplet become highly dilute. Using approximations for a dilute solute, the Köhler equation can be written as:[58]

$$\frac{p_w}{p_0} = \left(1 - \frac{3n_s M_w}{4\pi\rho_w r^3}\right) \times \exp\left(\frac{2\sigma_w M_w}{RT\rho_w r}\right). \quad (6)$$

In eqn (6), σ_w is the surface tension of water, M_w is the molar mass of water, n_s is the number of moles of dissolved solute, and ρ_w is the density of water. The saturation ratio can also be converted to a percent supersaturation (SS):

$$SS = 100\% \times \left(\left(\frac{p_w}{p_0}\right) - 1\right). \quad (7)$$

In all Köhler calculations, no change in volume upon mixing of solutes and water was assumed during hygroscopic growth. The increased droplet volume at each calculated radius was taken to be the volume of water in the droplet (*i.e.*, the total

Table 2 Mass fraction of surfactants in dry particles of different radii. Low, medium, and high mass fractions correspond to the size-dependent organic mass fractions determined by Kleinheins *et al.*[22]

Dry radius	Low	Medium	High
25 nm	0.689	0.930	0.988
50 nm	0.522	0.898	0.957
100 nm	0.386	0.667	0.864

droplet volume was the sum of the volume of the dry aerosol particle and the water added due to hygroscopic growth). All solutes were assumed to be nonvolatile.

Köhler calculations were performed for a range of dry radii between 25 nm and 100 nm and for different mass ratios of surfactants and NaCl in the dry particle (Table 2). In each instance, the dilute solute approximation is compared to calculations accounting for surfactant partitioning, utilizing both subgroup descriptions for AIOMFAC predictions of water activity. The point of cloud droplet activation for each case (critical radius, r_{crit} and critical supersaturation, SS_{crit}) is determined by finding the maximum of the calculated Köhler curve.

Dilute solute approximation. Eqn (6) was used to calculate Köhler curves using the dilute solute approximations. The number of moles of each component (surfactant and NaCl) in a dry particle was calculated using a linear combination of molar volumes, calculated from the pure (dry) component densities and molecular masses provided in Table 3 and the dry particle volume, assuming a spherical geometry. All solutes were assumed to be dissolved in the droplet interior, and the moles of dissolved ions and surfactant were used to determine the contribution to the moles of solute (n_s). Physical parameters of water used in the calculations are provided in Table 3.

Surfactant partitioning. Due to the large surface-area-to-volume ratio of aerosol droplets, surfactants can undergo bulk concentration depletion as they partition to maintain equilibrium between the droplet bulk and surface. The impact of surfactant partitioning on both the droplet surface tension and its water activity was explored using eqn (5). Here, the effective bulk surfactant concentration, accounting for the size- and concentration-dependent surfactant partitioning, was calculated at each step using eqn (2)–(4). The calculated effective bulk concentration was also used in eqn (1) to determine the droplet's surface tension. If the calculated surface tension is lower than the minimum surface tension (*i.e.*, the droplet bulk is above the surfactant's CMC), then it is replaced with the minimum surface tension value in Table 1.

Table 3 Physical parameters for solution components

Component	Molar mass (g mol^{-1})	Pure component (dry) density (g cm^{-3})	O : C ratio
Water	18.01528	0.998	—
NaCl	58.443	2.170	—
Triton X-100	647	1.070	0.34
Tween20	1226	1.100	0.49

The effective bulk concentration was also used to determine the surfactant mass fraction in the droplet bulk. This mass fraction, in addition to the NaCl mass fraction, was used to determine the droplet's water activity from both of the oxyethylene and ether–alkyl subgroup description interpolations (Fig. S2).

Using the ether–alkyl group description, AIOMFAC sometimes predicts water activities greater than unity when the surfactant mass fraction is high (Fig. S2A/C). These unphysical water activities suggest that a liquid–liquid phase separation is likely a thermodynamically stable state.[59] In eqn (5), the water activity must be less than or equal to one. Two different assumptions for the evolution of water activity when water activities greater than unity are predicted are compared.

Liquid–liquid phase separation. First, it was assumed that a liquid–liquid phase separation (LLPS) occurs when the water activity is greater than one, which is sometimes the case using the alkyl–ether subgroup approach to describe mixtures that include PEG-like units.[50] A water activity greater than unity is unphysical. If the online version of AIOMFAC predicts water activity greater than unity, this suggests that a liquid–liquid phase separation is likely a thermodynamically stable state, although the online AIOMFAC model does not explicitly solve for this state.[50,59] When LLPS is predicted, the surfactant is removed from the bulk solution, and the water activity of the droplet was recalculated using only the mass fraction of NaCl. If LLPS occurs, the surface tension of the droplet could also be impacted. At each instance where the water activity is greater than unity, we also calculate the fractional surface coverage of the droplets using the area covered by a monolayer of the surfactant and the surface area of the droplet (eqn (8)).

$$\text{Surface coverage} = \frac{\text{total moles of surfactant} \times \Gamma_{max}}{4\pi r^2} \quad (8)$$

When phase separation occurs before the critical radius, there was always sufficient surfactant for a full surface coverage, and the surfactant partitioning model already predicted that the droplet surface tension was at its minimum value. Phase separation was also predicted after droplet activation. Varying the surface tension in this region has no impact on the activation barrier. Additionally, the surface coverage was generally below 10% in this region, which is not sufficient to significantly reduce the droplet surface tension from that of water.

Lowest water activity. Second, if AIOMFAC predicts water activity greater than unity during hygroscopic growth, it was assumed that the water activity of the droplet can be described by the lower of the ether–alkyl–NaCl and NaCl only water activity interpolations. This is similar to the approach previously used when AIOMFAC predictions of water activity have been used in Köhler calculations.[22]

Results and discussion

The impact of nonionic surfactants on water activity during hygroscopic growth and how different assumptions alter predictions of cloud droplet activation is investigated. Nonionic

surfactants Triton X-100 and Tween20 were selected due to their similarity in concentration required to reduce the surface tension of bulk solutions, the minimum surface tension that can be reached at full surface coverage, and the oxygen to carbon (O : C) ratios to surfactants found in the sea surface microlayer and sea spray aerosol.[12,14–16,36,60–62] Table 3 shows the O : C ratios for Triton X-100 and Tween20. Additionally, recent work showed that the water activity predicted by AIOMFAC for surfactants with PEG-like tails is significantly different depending on whether the tails are modeled as ether and alkyl groups or oxyethylene groups.[50] Since both these molecules contain PEG-like chains, they provide model systems with which to test the importance of an accurate description of water activity in predicting cloud droplet activation for surfactant-containing aerosols. NaCl is selected as a cosolute as much of the field work identifying surfactants in aerosols has been focused on sea spray, and NaCl is the major salt in seawater.[63]

The mass fraction of organics in dry aerosol can vary with aerosol size, formation pathway, and location. Kleinheins *et al.*[22] compiled data from field measurements to determine the size-dependent organic mass fraction,[64–66] providing bounds for low and high organic content.[22] Here, the size-dependent low, medium, and high organic mass fractions are used in Köhler calculations. Fig. 1 shows the size-dependent solute concentrations, surface tension, and equilibrium saturation ratio for 100 nm dry radius aerosol particles containing NaCl and low, medium, or high organic fractions composed of Tween20. Panels A–C show the size-dependent solute concentration. NaCl and the bulk concentration of Tween20 decrease steadily as the droplet undergoes hygroscopic growth. The bulk Tween20

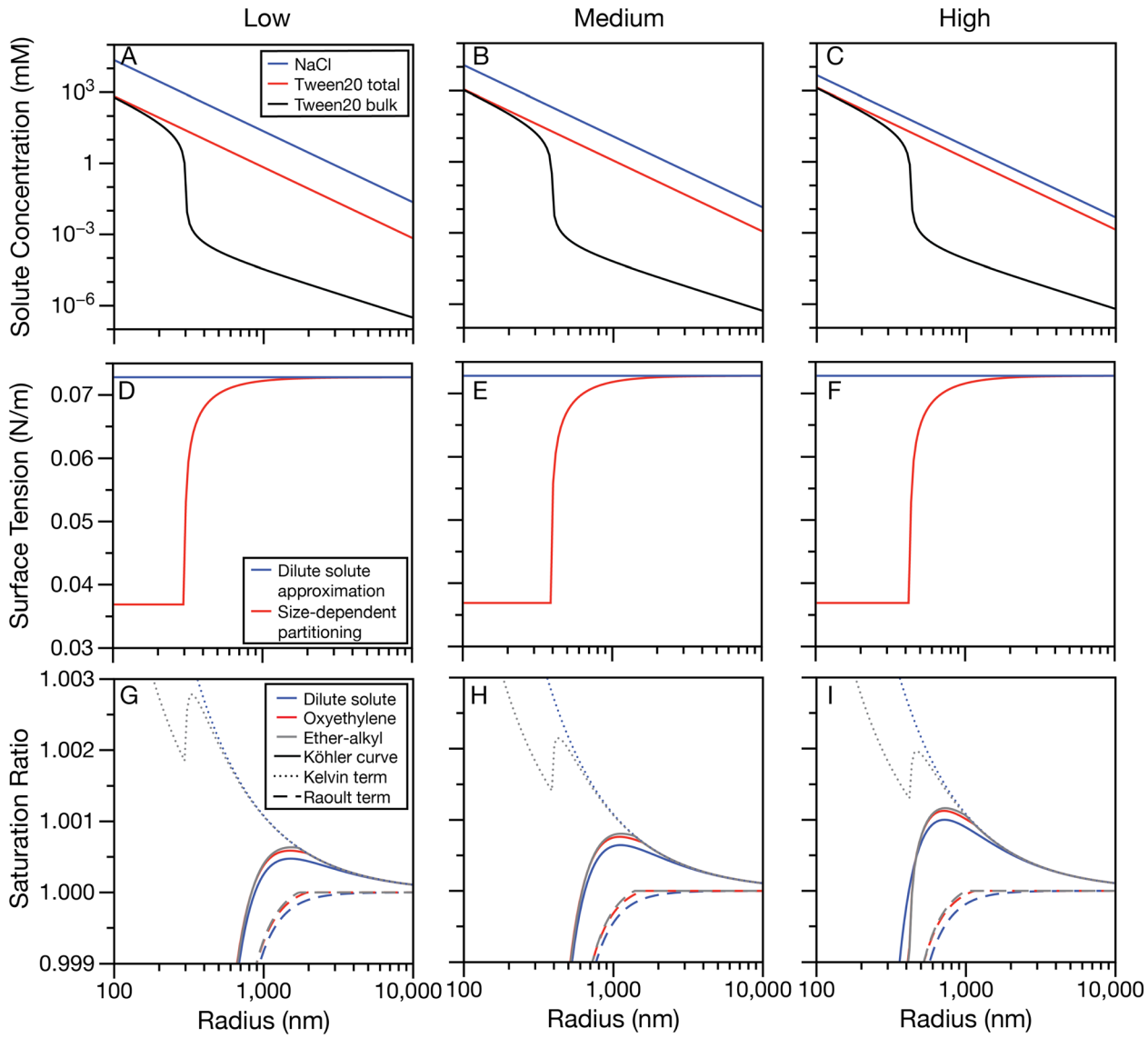

Fig. 1 Solute concentration (A–C), surface tension (D–F), and saturation ratio (G–I) for 100 nm dry radius particles containing low (column 1, $w_{org} = 0.386$), medium (columns 2, $w_{org} = 0.667$), and high (column 3, $w_{org} = 0.864$) Tween20 mass fractions. Köhler curves are calculated using the dilute solute approximation as well as using the AIOMAC activity interpolations using the oxyethylene and ether–alkyl subgroup descriptions. The contribution from the Kelvin term is the same for both subgroup descriptions of water activity.

concentration includes the size- and concentration-dependent surfactant partitioning and shows a steep drop in bulk concentration as bulk-to-surface partitioning becomes significant. This onset of bulk surfactant depletion depends both on the dry size and total surfactant concentration. In Fig. 1, the drop in bulk Tween20 concentration moves to larger radii as the organic fraction is increased from the low scenario to the high scenario. The surface tension accounting for bulk-to-surface partitioning is determined using the simple kinetic partitioning model and shown in panels D–F. Due to the difference in size during hygroscopic growth when bulk depletion becomes significant, there is also a shift towards larger wet radii when the surface tension begins to increase from its minimum value from low to high organic fractions. Using the dilute solute approximation, the surface tension of pure water is used throughout hygroscopic growth and is also shown in panels D–F.

Fig. 1 panels G–I show the equilibrium saturation ratio as a function of wet radius using three different assumptions: (1) dilute solute approximation, (2) surfactant partitioning where the water activity term is calculated with AIOMFAC using oxyethylene subgroups, and (3) surfactant partitioning where the water activity term is calculated with AIOMFAC using ether and alkyl subgroups. These panels also show the contribution from the Kelvin and Raoult terms to the overall Köhler curve. The Kelvin term calculated using surfactant partitioning shows a unique shape compared to that using the dilute solute approximation, owing to the changing surface tension during hygroscopic growth. Note that the surfactant partitioning is only treated with the simple kinetic model and is identical for oxyethylene and ether–alkyl subgroup descriptions of water activity. In panels G and H, since the Kelvin term contributions at radii near the critical radius are generally the same with and without including surfactant partitioning, the differences in critical saturation ratio can be attributed to the Raoult effect. In panel I, the difference in hygroscopic growth cases can be attributed to both the Kelvin and Raoult terms. The difference in the Kelvin term between the dilute solute approximation and including surface partitioning is substantial in the region near the cloud droplet activation barrier. The Raoult term contributions also show small differences in this region. Again, the difference between the two methods of calculating water activity in AIOMFAC is small compared to using the dilute solute approximation, which assumes all components are completely soluble.

Fig. S3–S7 show similar plots for Tween20 in 50 nm and 25 nm dry radius particles and Triton X-100 in 100 nm, 50 nm and 25 nm dry radius particles. Generally, the trends that are observed in Fig. 1 hold for both surfactants. The largest differences between the dilute solute approximation and accounting for bulk-to-surface partitioning are observed for droplets with a high organic fraction, and the largest difference in the Raoult contribution between the oxyethylene and ether–alkyl subgroup descriptions occurs for 100 nm dry radius particles (Table S1).

For some combinations of surfactant, dry radius, and surfactant mass fraction, two peaks are observed in the Köhler curve (*e.g.*, Fig. S3I, S4I, S6I, S7H, and S7I). This feature is due to a discontinuity in the size- and composition-dependent water activity. Using the ether–alkyl subgroup description, AIOMFAC can predict a water activity greater than unity (Fig. S2). The onset of this nonphysical water activity prediction has been previously shown to be close to, but not necessarily coincident with, the CMC of the surfactant. Furthermore, AIOMFAC does not predict water activity greater than unity at every surfactant mass fraction greater than the CMC.[50] Since a water activity greater than one is not realistic, two strategies are employed to calculate the water activity in this case. In Fig. S3I, S4I, S6I, S7H, and S7I, a LLPS assumption was employed. Under this assumption, when the water activity is greater than one, a purely organic layer has formed on top of an aqueous NaCl layer, and the water activity is calculated from AIOMFAC using only NaCl as the solute. At some composition, AIOMFAC predicts the solution to become homogeneous again, and the water activity for the ternary mixture is again used. Fig. S8 shows an example of the resulting water activity curve. At this transition, there is often a discontinuity in water activity (following the solid black in Fig. S8). The second assumption (lowest) calculates the water activity of a solution containing NaCl only as well as the ternary mixture at every point and uses the lowest water activity (following the dotted black line in Fig. S8, a similar procedure to that of Kleinheins *et al.*[22]). This method also assumes that the water activity of the droplet can be approximated by the water activity of a droplet containing only NaCl (as the surfactant has been removed to a surface layer), but it removes the discontinuity resulting from switching between the NaCl-only and ether–alkyl–NaCl water activity interpolations. While this method generally provides a smoother transition between the two cases, there can still be a small bump in water activity where the transition occurs between using the binary and ternary descriptions of water activity. Fig. S8 shows an example of the size-dependent water activity, in the region near the discontinuity, using these two assumptions. Using the oxyethylene subgroup description, the water activity does not exceed unity at the level of precision of the interpolation, and the LLPS and lower assumptions for size- and composition-dependent water activity do not need to be employed; rather, the water activity can be directly taken from the interpolation.

Fig. 2 shows all the Köhler curves for 25, 50, and 100 nm dry radius particles with low, medium, and high Tween20 mass fractions. Here, the dilute solute approximation (fully dissolved solute) is compared to the oxyethylene subgroup description as well as the ether–alkyl subgroup description using the LLPS and lower assumptions to calculate water activity. In panel A for 25 nm dry radius particles, the predicted LLPS and the lowest water activity methods follow the same trend. Although the entire ether–alkyl curve is not identical to the oxyethylene description of water activity, the region near cloud droplet activation is identical for all three methods of describing water activity. In panel B for 50 nm dry radius particles, the LLPS and lowest water activity descriptions show different behavior around a 100 nm wet radius. The LLPS method shows a sharp spike in supersaturation, while the lowest method shows a small kink in the curve. This indicates that this sharp feature is a result of the transition between descriptions of water

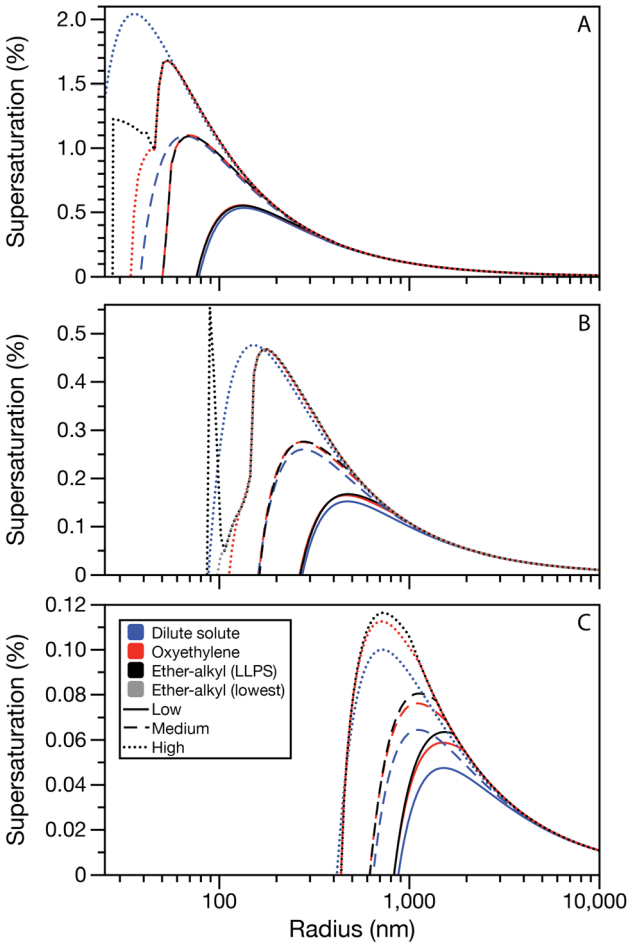

Fig. 2 Köhler curves for particles with dry radii of (A) 25 nm, (B) 50 nm and (C) 100 nm and low, medium, and high Tween20 mass fractions (Table 1). The water activity for the ether–alkyl subgroup description is shown using both the LLPS assumption and the lowest water activity assumption, where the calculated water activity goes above unity at any point during activation (*e.g.*, 50 nm high).

activity. Since LLPS was not observed by Werner *et al.* in the region where AIOMFAC predictions are greater than unity,[50] this feature is unlikely to limit cloud droplet activation in the case where it reaches higher supersaturations than the second broader peak in the curve. Fig. S9 shows a similar result for Triton X-100. Generally, although the LLPS and lowest assumptions used to handle water activities greater than unity can lead to different behavior at small radii, the main, broader feature of the Köhler curve is identical between the two assumptions.

Fig. 2 also shows that differences between the dilute solute approximation and surfactant partitioning impact on water activity depend on droplet size. For the smallest droplets in panel A, including surfactant partitioning decreases the supersaturation barrier to cloud droplet activation. This is also observed in panel B, where the difference in activation barrier is smaller. However, in panel C for the largest droplets, the trend is inverted, and the supersaturation barrier is lower using the dilute solute approximation than when accounting for surfactant partitioning. This overall trend is also observed in Fig. S9 for Triton X-100. This shift from surfactant lowering the barrier to cloud droplet activation compared to the dilute solute approximation for smaller droplets, but increasing the barrier for larger droplets, is due to the combined effects that surfactant partitioning has on aerosol surface tension and water activity, with the Kelvin term dominating at smaller dry particle sizes and the Raoult term dominating at larger dry particle sizes.

To understand how accurate these size- and organic mass fraction-predictions of CCN activation are, predicted critical supersaturations are compared to CCN measurements for aerosols containing Triton X-100 and NaCl. The dry radii at which 50% of particles underwent cloud droplet activation at a given level of supersaturation, measured by Petters and Petters,[12,67] are shown in Fig. 3. These data are overlaid on predictions of critical supersaturation for a range of dry radii and volume fractions of NaCl. Panel A shows the oxyethylene subgroup description for water activity, and panel B shows the lowest ether–alkyl subgroup water activity. Fig. S10 shows the CCN data compared to the dilute solute approximation and the LLPS ether–alkyl subgroup water activity description. In all cases, there is good agreement when the volume fraction of NaCl is near one, since low surfactant concentrations do not greatly impact the surface tension or water activity under dilute conditions. As the NaCl volume fraction decreases to about 0.6–0.4, there is generally an underprediction of critical supersaturation by the model compared to the observations. However,

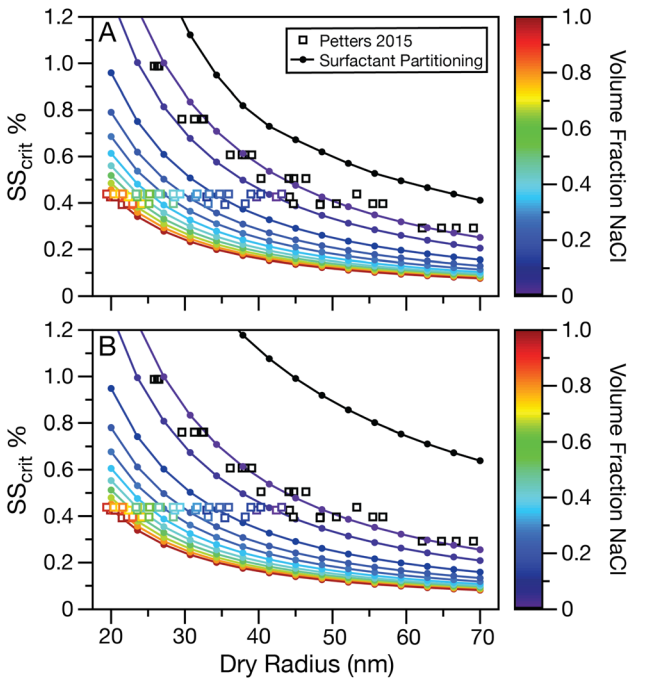

Fig. 3 Critical supersaturation (SS_{crit}) predicted using Köhler theory with size- and composition-dependent surfactant partitioning using (A) the oxyethylene subgroup and (B) the ether-alkyl subgroups (lowest water activity) to determine droplet water activity. CCN measurements from Petters 2015 are overlaid.[12,67]

there is again good agreement between the model and measurements when the volume fraction of NaCl reaches the 0.3–0.2 range. The different water activity assumptions show small differences in critical supersaturation as a function of NaCl volume fraction and size, but these differences are small compared to the variation in the experimental data. The largest difference in size-dependent critical supersaturation predictions occurs when the NaCl volume fraction is zero (*i.e.*, pure surfactant particles). These differences are quantified using the root mean square error calculated from the difference between the experimental CCN measurements at the radius where 50% of the particles activate and the Köhler prediction for the critical supersaturation at that dry radius using different assumptions for water activity during hygroscopic growth. While none of the pure surfactant predictions overlap with the experimental observations, the oxyethylene subgroup description shows the closest agreement (root mean square error between the CCN data and model is 2.4%). Both the ether–alkyl subgroup methods show very poor agreement with the experimental data (root mean square error is 10.3%). Using the dilute solute approximation, the root mean square error between the CCN data and model predictions is 3.9%. This observation further motivates the use of the oxyethylene group for molecules that have PEG-like tails. Still, the overprediction of critical supersaturation for pure surfactant particles shows that the fundamental understanding of the impact of surfactants on cloud droplet activation is still incomplete. Additional CCN activation datasets for strong surfactants and their mixtures with salts to validate the existing data would aid this understanding.

Finally, the impact of atmospheric supersaturation on the fraction of aerosol activated into cloud droplets is explored. Fig. 4 shows a simulated sea spray aerosol size distribution containing an ultrafine mode, a combined Aitken/accumulation mode, and a coarse mode, based on observations from Bates *et al.*[68] Köhler calculations are performed assuming the size-dependent high organic mass fraction, and the dilute solute approximation (dotted vertical lines) is compared to surfactant partitioning and water activity predicted using the oxyethylene subgroup in AIOMFAC (vertical dashed lines). At a 0.1% supersaturation level, only the largest particles are predicted to activate, and as seen in Fig. 2, including surfactant partitioning slightly decreases the number of particles that are expected to activate. As the ambient supersaturation level is increased to 0.5%, the lower limit of the particles that are expected to activate gets smaller, and a crossover point is reached, where the dilute solute approximation and accounting for surfactant partitioning predict the same cut-off for cloud droplet activation. As the ambient supersaturation is further increased to 1%, now more than 50% of the Aitken/accumulation mode particles are predicted to activate, and accounting for surfactant partitioning predicts that smaller particles will activate than would be expected from the dilute solute approximation. Fig. 4 highlights why large differences between observed CCN concentrations and Köhler theory may be most noticeable for small size bins. The discrepancy between the dilute solute approximation and accounting for surfactant partitioning at supersaturation levels for the size where coarse mode particles activate does not greatly change the predicted number concentration of CCN. However, in this high surface active organic fraction example, at supersaturation levels around 1%, small changes in the minimum dry radius that will activate lead to large differences in CCN concentrations, as these radii are near the maximum number concentration of the Aitken/accumulation mode.

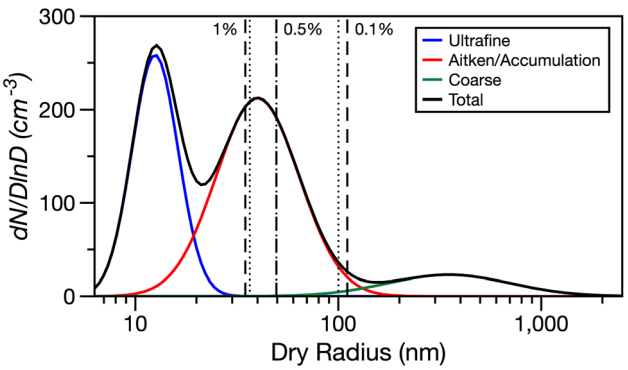

Fig. 4 Simulated sea spray aerosol size distribution based on observations from Bates *et al.*[68] Vertical dotted lines show the smallest dry radius that is predicted to activate at 1, 0.5, and 0.1% supersaturation using the dilute solute approximation, and the vertical dashed lines show the smallest dry radius that is predicted to activate when surfactant partitioning is included (oxyethylene subgroup for water activity). The size-dependent high organic mass fraction is used in all calculations.

Conclusion

Surfactant partitioning in aerosol droplets can impact both the droplet's surface tension and water activity. Under low nonionic surfactant fractions and small dry radii conditions, surfactant partitioning has little effect on either the Kelvin or Raoult term and the dilute solute approximation provides nearly the same results as including surfactant partitioning (including any description of aerosol water activity). For high organic fractions, including surfactant partitioning predicts a higher supersaturation barrier for the smallest dry radius particles compared to the dilute solute approximation, but a lower supersaturation barrier for the largest dry radius particles. These differences in aerosol size are due to the combined differences in both the Kelvin and Raoult terms, with surface tension dominating for smaller particles and water activity dominating for larger particles.

Using ether and alkyl subgroups to describe the PEG-like tail of these surfactants leads to AIOMFAC predicting water activities greater than unity for some droplet compositions, which is unphysical and thus requires making an assumption about the droplet morphology and its impact on water activity. Accounting for surfactant partitioning and using the oxyethylene subgroup description for droplet water activity provides the closest agreement with CCN measurements of Triton X-100 and NaCl mixtures reported in the literature,[12,67] further motivating its use to describe water activity for molecules containing a PEG-like tail. However, for particles containing only Triton X-100, the critical supersaturation is overpredicted. This overprediction

indicates that there is still an incomplete understanding of the impact of strong nonionic surfactants on surface tension and water activity in high surface-area-to-volume ratio droplets. Additional CCN measurements for strong surfactants and their mixtures with salts, and measurement–model comparisons for aerosols containing pure surfactants and high surfactant fractions, may elucidate the reasons for these discrepancies. Furthermore, additional improvements to the description of water activity for aqueous strong surfactants using hygroscopic growth data could improve CCN predictions for pure nonionic surfactant particles. Finally, ambient aerosols contain a mixture of nonionic and ionic surfactants. Although AIOMFAC does not include charged organic groups, a similar interpolation approach could be used to describe water activity during hygroscopic growth if water activities were measured across the full composition space.

Conflicts of interest

There are no conflicts to declare.

Data availability

Data underlying this work is available on Oregon State University's Scholar Archive, https://doi.org/10.7267/xp68kr421.

Supplementary information (SI) is available. See DOI: https://doi.org/10.1039/d6ea00035e.

Acknowledgements

AB acknowledges the National Science Foundation (NSF) for financial support through award number 2503671.

Notes and references

1 D. K. Farmer, C. D. Cappa and S. M. Kreidenweis, *Chem. Rev.*, 2015, **115**, 4199–4217.
2 G. McFiggans, P. Artaxo, U. Baltensperger, H. Coe, M. C. Facchini, G. Feingold, S. Fuzzi, M. Gysel, A. Laaksonen, U. Lohmann, T. F. Mentel, D. M. Murphy, C. D. O'Dowd, J. R. Snider and E. Weingartner, *Atmos. Chem. Phys.*, 2006, **6**, 2593–2649.
3 N. Good, D. O. Topping, J. D. Allan, M. Flynn, E. Fuentes, M. Irwin, P. I. Williams and H. Coe, *Atmos. Chem. Phys.*, 2010, **10**, 3189–3203.
4 M. Irwin, N. Good, J. Crosier, T. W. Choularton and G. Mcfiggans, *Atmos. Chem. Phys.*, 2010, **10**, 11737–11752.
5 J. Ovadnevaite, A. Zuend, A. Laaksonen, K. J. Sanchez, G. Roberts, D. Ceburnis, S. Decesari, M. Rinaldi, N. Hodas, M. C. Facchini, J. H. Seinfeld and C. O'Dowd, *Nature*, 2017, **546**, 637–641.
6 F. Bi, G. Lin, T. Fan, Y. Li, X. Guo and C. Wu, *Geophys. Res. Lett.*, 2025, **52**, e2025GL118598.
7 B. Graham, O. L. Mayol-Bracero, P. Guyon, G. C. Roberts, S. Decesari, M. C. Facchini, P. Artaxo, W. Maenhaut, P. Köll and M. O. Andreae, *J. Geophys. Res.: Atmos.*, 2002, **107**, 8047.
8 S. Decesari, S. Fuzzi, M. C. Facchini, M. Mircea, L. Emblico, F. Cavalli, W. Maenhaut, X. Chi, G. Schkolnik, A. Falkovich, Y. Rudich, M. Claeys, V. Pashynska, G. Vas, I. Kourtchev, R. Vermeylen, A. Hoffer, M. O. Andreae, E. Tagliavini, F. Moretti and P. Artaxo, *Atmos. Chem. Phys.*, 2006, **6**, 375–402.
9 K. A. Prather, T. H. Bertram, V. H. Grassian, G. B. Deane, M. D. Stokes, P. J. DeMott, L. I. Aluwihare, B. P. Palenik, F. Azam, J. H. Seinfeld, R. C. Moffet, M. J. Molina, C. D. Cappa, F. M. Geiger, G. C. Roberts, L. M. Russell, A. P. Ault, J. Baltrusaitis, D. B. Collins, C. E. Corrigan, L. A. Cuadra-Rodriguez, C. J. Ebben, S. D. Forestieri, T. L. Guasco, S. P. Hersey, M. J. Kim, W. F. Lambert, R. L. Modini, W. Mui, B. E. Pedler, M. J. Ruppel, O. S. Ryder, N. G. Schoepp, R. C. Sullivan and D. Zhao, *Proc. Natl. Acad. Sci. U. S. A.*, 2013, **110**, 7550–7555.
10 A. L. Bondy, D. Bonanno, R. C. Moffet, B. Wang, A. Laskin and A. P. Ault, *Atmos. Chem. Phys.*, 2018, **18**, 12595–12612.
11 A. Kroflič, S. Frka, M. Simmel, H. Wex and I. Grgić, *Environ. Sci. Technol.*, 2018, **52**, 9179–9187.
12 S. S. Petters and M. D. Petters, *J. Geophys. Res.: Atmos.*, 2016, **121**, 1878–1895.
13 K. A. Wokosin, E. L. Schell and J. A. Faust, *Environ. Sci.: Atmos.*, 2022, **2**, 775–828.
14 V. Gérard, B. Nozière, C. Baduel, L. Fine, A. A. Frossard and R. C. Cohen, *Environ. Sci. Technol.*, 2016, **50**, 2974–2982.
15 V. Gérard, B. Nozière, L. Fine, C. Ferronato, D. K. Singh, A. A. Frossard, R. C. Cohen, E. Asmi, H. Lihavainen, N. Kiveka, M. Aurela, D. Brus, S. Frka and A. C. Kusan, *Environ. Sci. Technol.*, 2019, **53**, 12379–12388.
16 A. A. Frossard, V. Gérard, P. Duplessis, J. D. Kinsey, X. Lu, Y. Zhu, J. Bisgrove, J. R. Maben, M. S. Long, R. Y. Chang, S. R. Beaupré, D. J. Kieber, W. C. Keene, B. Nozière and R. C. Cohen, *Environ. Sci. Technol.*, 2019, **53**, 9047–9417.
17 A. M. Deegan, C. K. Glenn, O. E. Hajj, A. Anosike, K. Kumar, M. Abdurrahman, B. Bai, P. Liu, J. O'Brien, R. Saleh and A. A. Frossard, *ACS ES&T Air*, 2025, **2**, 264–276.
18 A. N. Schwier, N. Sareen, D. Mitroo, E. L. Shapiro and V. F. McNeill, *Environ. Sci. Technol.*, 2010, **44**, 6174–6182.
19 P. K. Quinn, T. S. Bates, K. S. Schulz, D. J. Coffman, A. A. Frossard, L. M. Russell, W. C. Keene and D. J. Kieber, *Nat. Geosci.*, 2014, **7**, 228–232.
20 T. C. Burdette, R. L. Bramblett, A. M. Deegan, N. R. Coffey, A. S. Wozniak and A. A. Frossard, *ACS Earth Space Chem.*, 2022, **6**, 2929–2943.
21 E. K. Werner, M. Hammond and A. Bain, *Aerosol Sci. Technol.*, 2025, **59**, 781–793.
22 J. Kleinheins, N. Shardt, U. Lohmann and C. Marcolli, *Atmos. Chem. Phys.*, 2025, **25**, 881–903.
23 N. L. Prisle, *Atmos. Chem. Phys.*, 2021, **21**, 16387–16411.
24 N. L. Prisle, T. Raatikainen, R. Sorjamaa, B. Svenningsson, A. Laaksonen and M. Bilde, *Tellus Ser. B Chem. Phys. Meteorol.*, 2008, **60 B**, 416–431.
25 S. Vepsäläinen, S. M. Calderón, J. Malila and N. L. Prisle, *Atmos. Chem. Phys.*, 2022, **22**, 2669–2687.
26 S. Vepsäläinen, S. M. Calderón and N. L. Prisle, *Atmos. Chem. Phys.*, 2023, **23**, 15149–15164.

27 J. J. Lin, J. Malila and N. L. Prisle, *Environ. Sci.: Processes Impacts*, 2018, **20**, 1611–1629.
28 J. J. Lin, T. B. Kristensen, S. M. Calderón, J. Malila and N. L. Prisle, *Environ. Sci.: Processes Impacts*, 2020, **22**, 271–284.
29 J. Malila and N. L. Prisle, *J. Adv. Model. Earth Syst.*, 2018, **10**, 3233–3251.
30 R. Schmedding and A. Zuend, *Atmos. Chem. Phys.*, 2023, **23**, 7741–7765.
31 B. Nozière, C. Baduel and J. L. Jaffrezo, *Nat. Commun.*, 2014, **5**, 1–7.
32 S. D. Forestieri, S. M. Staudt, T. M. Kuborn, K. Faber, C. R. Ruehl, T. H. Bertram and C. D. Cappa, *Atmos. Chem. Phys.*, 2018, **18**, 10985–11005.
33 N. Ferdousi-Rokib, K. A. Malek, I. Mitchell, L. M. Fierce and A. A. Asa-Awuku, *ACS ES&T Air*, 2025, **2**, 1454–1467.
34 B. R. Bzdek, J. P. Reid, J. Malila and N. L. Prisle, *Proc. Natl. Acad. Sci. U. S. A.*, 2020, **117**, 8335–8343.
35 A. Bain, N. L. Prisle and B. R. Bzdek, *ACS Earth Space Chem.*, 2024, **8**, 2244–2255.
36 A. Bain, K. Ghosh, N. L. Prisle and B. R. Bzdek, *ACS Cent. Sci.*, 2023, **9**, 2076–2083.
37 A. Bain, K. Ghosh, K. Tumashevich, N. L. Prisle and B. R. Bzdek, *Atmos. Chem. Phys.*, 2025, **25**, 5633–5645.
38 K. L. Ramos, E. K. Werner, B. R. Bzdek and A. Bain, *Environ. Sci. Technol.*, 2025, **59**, 18761–18770.
39 M. I. Jacobs, M. N. Johnston and S. Mahmud, *J. Phys. Chem. A*, 2024, **128**, 9986–9997.
40 V. Shahabadi, C. Lefort, H. T. Law, M. N. Chan and T. C. Preston, *Atmos. Chem. Phys.*, 2025, **25**, 14301–14313.
41 A. Bain, L. Lalemi, N. C. Dawes, R. E. Miles, A. M. Prophet, K. R. Wilson and B. R. Bzdek, *J. Am. Chem. Soc.*, 2024, **146**, 16028–16038.
42 R. Sorjamaa, B. Svenningsson, T. Raatikainen, S. Henning, M. Bilde and A. Laaksonen, *Atmos. Chem. Phys.*, 2004, **4**, 2107–2117.
43 B. E. Swanson and A. A. Frossard, *Aerosol Sci. Technol.*, 2023, **57**, 63–76.
44 A. A. Frossard, W. Li, V. Gérard, B. Nozière and R. C. Cohen, *Aerosol Sci. Technol.*, 2018, **52**, 459–469.
45 R. L. Bramblett and A. A. Frossard, *J. Phys. Chem. A*, 2022, **126**, 8695–8710.
46 C. W. Harmon, R. L. Grimm, T. M. McIntire, M. D. Peterson, B. Njegic, V. M. Angel, A. Alshawa, J. S. Underwood, D. J. Tobias, R. B. Gerber, M. S. Gordon, J. C. Hemminger and S. A. Nizkorodov, *J. Phys. Chem. B*, 2010, **114**, 2435–2449.
47 A. Alshawa, O. Dopfer, C. W. Harmon, S. A. Nizkorodov and J. S. Underwood, *J. Phys. Chem. A*, 2009, **113**, 7678–7686.
48 M. D. Petters and S. M. Kreidenweis, *Atmos. Chem. Phys.*, 2006, **7**, 1961–1971.
49 N. Hodas, A. Zuend, K. Schilling, T. Berkemeier, M. Shiraiwa, R. C. Flagan and J. H. Seinfeld, *Atmos. Chem. Phys.*, 2016, **16**, 12767–12792.
50 E. K. Werner, O. Wasserlein, C. Mahan, A. Zuend and A. Bain, *Phys. Chem. Chem. Phys.*, 2026, **28**, 6171–6180.
51 T. B. Kristensen, N. L. Prisle and M. Bilde, *Atmos. Res.*, 2014, **137**, 167–175.
52 C. Zhang, L. Bu, F. Fan, N. Ma, Y. Wang, Y. Yang, J. Größ, J. Yan and A. Wiedensohler, *Atmos. Environ.*, 2021, **266**, 118725.
53 J. Eastoe and J. S. Dalton, *Adv. Colloid Interface Sci.*, 2000, **85**, 103–144.
54 A. Zuend, C. Marcolli, B. P. Luo and T. Peter, *Atmos. Chem. Phys.*, 2008, **8**, 4559–4593.
55 A. Zuend, C. Marcolli, A. M. Booth, D. M. Lienhard, V. Soonsin, U. K. Krieger, D. O. Topping, G. McFiggans, T. Peter and J. H. Seinfeld, *Atmos. Chem. Phys.*, 2011, **11**, 9155–9206.
56 AIOMFAC Online Model, https://www.aiomfac.caltech.edu/model.html and https://aiomfac.lab.mcgill.ca, Last accessed: January 13, 2026.
57 N. J. Alvarez, M. Walker and S. L. Anna, *Soft Matter*, 2012, **8**, 8917–8925.
58 J. H. Seinfeld and S. N. Pandis, *Atmospheric Chemistry and Physics*, John Wiley & Sons, Inc., New Jersey USA, 2nd edn, 2006, pp. 769–770.
59 A. Zuend, in *Thermodynamics, Nonideal Mixing, and Phase Separation*, ed. D. Topping and M. Bane, John Wiley & Sons, Oxford, United Kingdom, 2022, ch. 3, pp. 78–132.
60 R. E. Cochran, O. Laskina, T. Jayarathne, A. Laskin, J. Laskin, P. Lin, C. Sultana, C. Lee, K. A. Moore, C. D. Cappa, T. H. Bertram, K. A. Prather, V. H. Grassian and E. A. Stone, *Environ. Sci. Technol.*, 2016, **50**, 2477–2486.
61 T. C. Burdette, R. L. Bramblett, K. Zimmerman and A. A. Frossard, *ACS Earth Space Chem.*, 2023, **7**, 1578–1591.
62 A. Zdziennicka, K. Szymczyk, J. Krawczyk and B. Jańczuk, *Fluid Phase Equilib.*, 2012, **318**, 25–33.
63 S. Gong, L. Barrie and M. Lazare, *J. Geophys. Res.: Atmos.*, 2002, **107**, 13–14.
64 C. D. O'Dowd, M. C. Facchini, F. Cavalli, D. Ceburnis, M. Mircea, S. Decesari, S. Fuzzi, Y. J. Yoon and J.-P. Putaud, *Nature*, 2004, **431**, 676–680.
65 M. C. Facchini, M. Rinaldi, S. Decesari, C. Carbone, E. Finessi, M. Mircea, S. Fuzzi, D. Ceburnis, R. Flanagan, E. D. Nilsson, G. de Leeuw, M. Martino, J. Woeltjen and C. D. O'Dowd, *Geophys. Res. Lett.*, 2008, **35**, L17814.
66 W. C. Keene, H. Maring, J. R. Maben, D. J. Kieber, A. A. Pszenny, E. E. Dahl, M. A. Izaguirre, A. J. Davis, M. S. Long, X. Zhou, L. Smoydzin and R. Sander, *J. Geophys. Res.: Atmos.*, 2007, **112**, D21202.
67 S. S. Petters, *On the Physicochemical Processes Controlling Organic Aerosol Hygroscopicity, PhD thesis*, North Carolina State University, 2015.
68 T. S. Bates, V. N. Kapustin, P. K. Quinn, D. S. Covert, D. J. Coffman, C. Mari, P. A. Durkee, W. J. De Bruyn and E. S. Saltzman, *J. Geophys. Res.: Atmos.*, 1998, **103**, 16369–16383.

